A Low-cost and Accurate Microwave Sensor System for Permittivity Characterization

Alireza Pourafzal*, *Student Member, IEEE,* Thomas Roi-Taravella, Michael Cheffena, and Sule Yildirim

***Abstract*— A novel low-cost microwave sensor system is proposed for accurate sensing of the real relative permittivity of materials under test (MUT). The proposed solution eliminates the need for using advanced measurement devices such as the vector network analyzer (VNA) for sensor characterization. The proposed sensor system is built on a software-defined radio platform. A suitable two-stage frequency estimation approach was developed for estimating the frequency shift of the resonator sensor associated with the real relative permittivity of the MUT. First, the neighborhood of the resonance frequency is obtained utilizing a low-resolution coarse search, followed by a fine search method to accurately estimate the resonance frequency. For the fine search, we modified the AM frequency estimation algorithm and the Golden Section search algorithm to suite the proposed sensor system. The performance of the proposed sensor system is validated through simulations and experiments. To demonstrate the feasibility of the concept, experiments were conducted by implementing the solution on a Universal Software Radio Peripheral transceiver using a resonator sensor for detecting the binary mixture of water and methanol. The results show that the proposed sensor system achieves measurement accuracy comparable to advanced equipment such as the VNA. Thus, the proposed sensor system could be a low-cost alternative for sensor characterization purposes with accuracy comparable to standard equipment.**

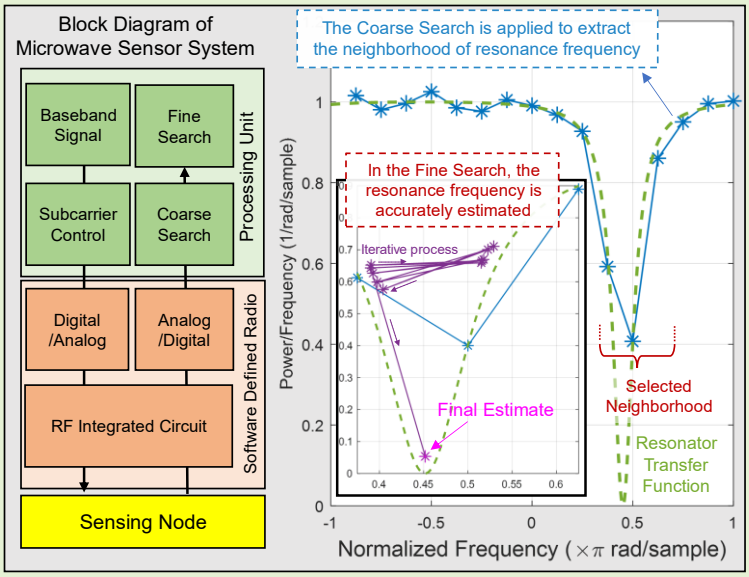

***Index Terms*—Microwave Sensors, Split Ring Resonators, Frequency Estimation, Software Defined Radio Systems**

I. Introduction

MICROWAVE sensors are realized as a large group of sensors fabricated complying with different requirements such as the desired Material Under Tests (MUTs), physical constraints, and sensor sensitivity [1]. Within the group of microwave sensors, resonance-based sensors can provide accurate measurements, as their resonance frequency is highly dependent on the dielectric characteristic of the resonator loaded to transmission line [2]. In this work, we focus on developing a sensor system for permittivity characterization based on Spilt Ring Resonators (SRR) [3]. This is due to SRR's simple and feasible structure while providing accurate performance in various sensing applications, such as biosensors and vital sign sensing [4-11] , non-intrusive liquid and mixture sensing [12-20], and solid and thickness sensing [20-23], just to name a few.

Interaction of the MUT with the sensing elements of such sensors changes their relative permittivity (ϵ_r) which affects the frequency behavior including the reflection (S_{11}) and transmission coefficients (S_{12}) [24]. To study these effects, it is common to apply the frequency-domain spectroscopy technique [25], in which, the resonance frequency, gain, and bandwidth of the resonator is measured to extract meaningful patterns associated with permittivity of the MUT.

Extracting these patterns can be quite challenging, especially when minimal variations appear in the MUT. In particular, for sensitive applications such as microfluid sensing [2, 16] and detecting small contamination in solutions [26, 27], the

The work was supported by the Research Council of Norway with grant no. 300989 (Corresponding author: Alireza Pourafzal).

Alireza Pourafzal and Michael Cheffena are with the Faculty of Engineering, Norwegian University of Science and Technology, 2815 Gjøvik, Norway (e-mails: alireza.pourafzal@ntnu.no and michael.cheffena@ntnu.no)

Thomas Roi-Taravella is with the National Graduate School of Engineering & Research Center, Caen, France (e-mail: thomas.roi-taravella@ecole.ensicaen.fr)

Sule Yildirim is with the Department of Computer Science, Norwegian University of Science and Technology, 2815 Gjøvik, Norway (e-mail: sule.yildirim@ntnu.no).

© 2022 IEEE. Personal use of this material is permitted. Permission from IEEE must be obtained for all other uses, in any current or future media, including reprinting/republishing this material for advertising or promotional purposes, creating new collective works, for resale or redistribution to servers or lists, or reuse of any copyrighted component of this work in other works

accuracy of the sensor depends on the high sensitivity of the sensing node ([28] and references within), and the resolution of measuring device.

A sensor with higher sensitivity, manifests a higher value of minimum frequency shift and broader range for the MUT's relative permittivity [29]. To study the factors which influence the sensitivity of a sensor, a detailed investigation on physics of SRRs is requisite. In [30], the physics of SRR and Complementary SRR (CSRR) structures are analyzed, and their equivalent-circuit models are obtained. In [31], the orientation of SRRs and their alignment to the host line axis is taken into consideration. Specifically, it is indicated that a modified model, which includes cross-polarization is required when the SRRs and CSRRs are rotated.

In [32], a highly sensitive sensor is developed in accordance with accurate physical-based modeling. The paper suggests investigating the electric field distribution in the resonance region, to achieve a more detailed equivalent-circuit model. Then, a novel sensor design is presented, considering the overall effective capacitance and inductance.

In [29], a comprehensive sensitivity analysis is carried out for a range of excitation schemes (from electric excitation to cross polarization excitation) and the order of CSRR design (single and double). Also, it is shown that thickness of substrate is another factor which should be considered for achieving the optimal sensitivity. Moreover, in [29] a general condition is presented in which the resonator exhibits a uniform sensitivity, regardless of the size of resonator and working frequency.

Slight changes in the MUT of highly sensitive sensing nodes [29, 32] will result in considerable frequency shifts, which can be simply detected in the measuring device. In addition, the fabrication of such sensors follows a low-cost and simple procedure. However, the extensive sensitivity analysis on the physics of the resonator and excitation scheme complicates the process of designing the sensor.

The other alternative is to employ a reliable and accurate measuring device, which supports different working frequencies and resolutions. Instruments like the Vector Network Analyzer (VNA) are commonly used as a measuring device for microwave sensors (especially during the development and testing phases of prototypes). They provide a broad frequency range (from Low Frequency band up to Super High Frequency band) and adequate dynamic range (the difference between maximum output power and noise floor level) for most sensing applications. In addition, some advanced models offer the frequency resolution as low as 1 Hz. In VNAs, due to the uniform sampling of the predefined frequency range, the measurement speed per sweep is inversely proportional to the resolution and frequency range. Consequently, high resolution sampling within a wide frequency range results in very long measurement cycles which is not preferred for sensing applications. Moreover, the output of VNA contains only implicit information (scattering-parameter data) regarding the MUT. Thus, offline post processing, such as regression analysis and classification, is necessary for such devices. Furthermore, the high price (especially for advanced models with high resolution) and bulky shape of VNAs restrict their availability to only Radio Frequency (RF) laboratories and projects with low budget margins.

In addition to VNA, alternative circuit designs can be utilized [5, 6, 33, 34]. In [5], an RF system is built utilizing two different SRRs. Finger touch on the surface of each SRR creates a distinct frequency shift which can be recognized using a commercial voltage-controlled-oscillator (VCO) and a simple RF power detector.

In [6], perturbation-injection-locked (PIL) sensor is designed using an active CSRR and an RF envelope detector. This design is advanced further in [7], where the envelop detector is substituted with a phase-locked-loop, which prevents mismatching between CSRR and the envelop detector.

In [33], the sensor is excited using a band pass signal generator covering the whole bandwidth, while on the output of the resonator a frequency comparator detects the variations between two parallel sensor circuits.

In [34], a wireless sensor system is developed. At the transmitter side, the antenna sensor acts as a load connected to the VCO. The VCO controls the carrier frequency of the transmitter, and any change in the dielectric properties of the MUT affects the impedance of the load and as a result, the carrier frequency. On the receiver side, the shift in carrier frequency is estimated using a simple zero-crossing algorithm. This design can be generalized for microwave sensors (such as SRR).

Alternative circuits are usually designed based on requirements such as resolution, bandwidth, and the frequency. And their performance is limited to the quality of the circuit components. This is preferred when an integrated resonator design is manufactured in large quantities and for commercial purposes. Nevertheless, the alternative circuits cannot be employed as a general tool for validating the performance of different sensors in the testing stage. For instance, when modifying the resonator in [6, 7, 34], a novel VCO circuit must be specifically designed, which appears as a nuisance parameter in sensitivity analysis of the sensor. Neglecting such a parameter can lead to unfair comparison between different designs.

Additionally, their final performance depends on the quality of equipment and implementation. This drawback is undesirable for highly sensitive sensors in the laboratory setting which require accurate measurements. Particularly, application of circuit design developed in [33] is confined to sensors with center frequency below 1 GHz and limited bandwidths. Moreover, commercial VCOs employed in [5] suffer from limited frequency shift steps which directly affect the accuracy of the sensor.

In [28], using an arbitrary wave generator (AWG), modulated orthogonal sequence codes are generated and given as the input of the resonator to extract the sensory information. This method mitigates the problem of the limited resolution of VNAs.

In [35-37] Software Defined Radio (SDR) systems are employed in RF sensing applications. In [35], an SDR system is developed to measure the permittivity of the MUT. The

Published version: https://doi.org/10.1109/JSEN.2022.3225662

system uses a simple coarse search with fixed step frequency which extracts the resonance frequency of the microwave sensor. In [36], it is shown that SDR systems can be applied as general tools for extracting the scattering parameters of the device under test. Moreover, in [37], an SDR-based sensor is developed, which enables applying proper waveform designs and time-frequency transformations for heartbeat motions detection.

Inspired by [35-37], we developed a stand-alone and low-cost sensor system which can provide online and accurate sensing of the real relative permittivity of the MUT. Such a system may eliminate the need for using expensive measurement devices (such as VNA and AWG) or designing alternative circuits during sensor development and testing phases in laboratories.

The rest of the paper is organized as follows. In section II, the proposed sensor system will be described. The system uses a novel measurement procedure to estimate the resonance frequency of the resonator. In section III, we analyze the theoretical foundation of the proposed procedure. Then, in section IV, the proposed sensor system along with the procedure for estimating the resonator's frequency is implanted in SDR platform where the real permittivity of the MUT is measured.

In section V, we carry out simulations to validate its performance. Specifically, the accuracy of resonance frequency estimation is compared with the accuracy of exhaustive search method in terms of frequency resolution, observation time, and bandwidth of the resonator. It is observed that for certain bandwidths (lower than 0.1π of the normalized frequency) the proposed procedure can improve the performance of exhaustive search up to hundred times, without adjusting the resolution and observation time.

To test the prototype, we set up an experiment for estimating the fraction of solute (methanol) in binary mixture of water and methanol. It is shown that the proposed sensor system can estimate the frequency and its associated real permittivity with the results comparable to advanced VNAs. Finally, in Section VI, we conclude the paper with advantages and drawbacks of the proposed sensor system.

II. Proposed Sensor System

The block diagram of the proposed sensor system is shown in Fig. 1. It consists of the MUT, a sensor, and a measuring device as described in the following.

A. The Material Under Test

The sensor system can detect changes in the real permittivity of the MUT in the near-field region (such as proximity, contact, and immersion). Thus, any modification on the MUT, which impacts on the dielectric properties of the material is recognized by the sensor. The long list of potential MUTs include but not limited to Thin-films, Paraffin, Teflon, Ethanol, Methanol, Glucose, Sodium Chloride, Oils, etc. In this paper, the binary mixture of Methanol/Water is employed as the MUT. Any change in the concentration of this solution affects the rotational diffusion of the polar molecules in the liquid, which results in dielectric change [38]. Therefore, we expect to observe shift in the resonance frequency of the resonator with changing of the fraction of the mixture.

B. The Sensing Node

The sensing node in the sensor system should be a frequency-variation sensor, including submersible sensors, microfluidic sensors, and bulk material sensors [1]. The transmission coefficients of such microwave structures indicate a narrowband sharp decrease centered at resonance frequency f_r and the bandwidth W_r. Note that the information related to the real permittivity of the MUT is embedded in f_r. Hence, the main goal is to estimate the frequency f_r.

C. Sensor data measuring device

Assume at the input port of the resonator (C1 in Fig. 1), we excite the resonator with a signal containing all the frequencies with identical power (e.g., flat spectral density). Then the output (C2) of the resonator contains minimum power at the resonance frequency f_r. This is because the energy of the signal at f_r is dispersed on the surface of the resonator.

Generating a signal with flat spectral density within a short interval can be realized using time-domain impulse signals. However, these transient signals deliver high energy in short time which can be harmful for commercial SDR transceivers. One practical solution is to apply an exhaustive search, in which, the measuring device excites all the frequencies one by one (known as frequency sweep). This method, which is used in VNAs, struggles with a trade-off between resolution and observation time.

Here, we propose a novel measurement procedure. The proposed procedure has two stages: first the whole specified bandwidth (W) will be explored with limited resolution

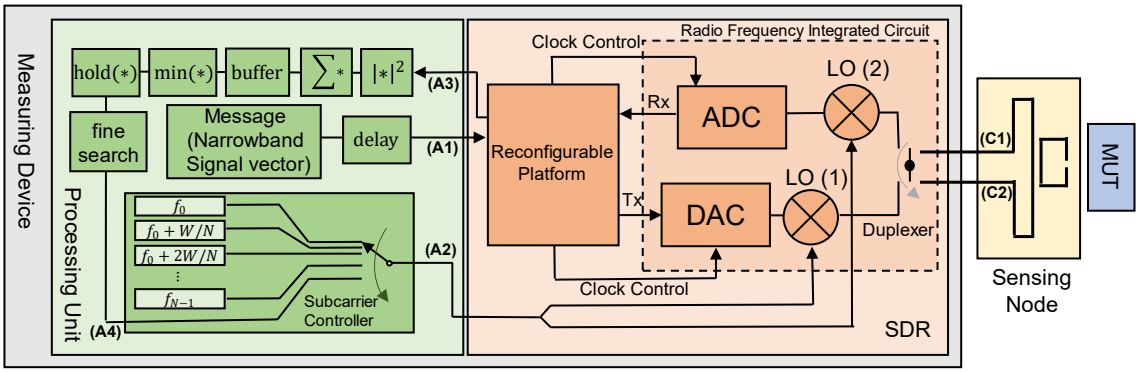

Fig. 1. Block Diagram of the proposed sensor system.

frequency sweep. This stage gives us a neighborhood of the resonance frequency (a frequency value close to the resonance frequency). Then in the fine search, we search the neighborhood until the estimation variance is lower than the user-defined threshold. The proposed procedure is executed in three consecutive steps, as follows.

1) *RF Signal Generation*

The role of this step is to excite the resonator at a specific frequency band. Inside the processing unit, a combination of samples of a deterministic signal with narrow bandwidth (the message) are generated. Then, they are combined as vector and given to the SDR system (A1). Simultaneously, a controller orders the SDR to transmit at a specific subcarrier (A2) associated with the buffer fullness level (see A3). The buffer has a size of N.

In the SDR system, the message (A1) is given to a reconfigurable platform (such as Field Programmable Gate Array (FPGA) or Digital Signal Processer (DSP)) for further processing [39]. It is worth mentioning that the configurable platforms inside the SDR transceivers are usually programmable. This offers the freedom to modify the bandwidth and sampling rate of the discrete signal. To adapt to such modifications the input of Digital-to-Analogue Converter (DAC) and output of Analogue-to-Digital Converter (ADC) should be synchronized (using clock control) with the rate of the DAC and ADC, respectively.

Within this platform, the discrete baseband signal is interpolated and digitally upconverted to intermediate frequency (IF), where the output (Tx in Fig. 1) is connected to the DAC inside the Radio-Frequency Integrated Circuit (RFIC). After DAC, a Local Oscillator (LO (1)) controlled by subcarrier controller (A2) upconverts the analog signal to RF level and transmits it through the resonator.

Due to the half-duplex structure assumed for the transceiver, the processing unit must wait for delay τ (necessary time for message transmission). Finally, the switch index of subcarrier controller is incremented. Until the buffer threshold exceeds, the same process will be iterated (coarse search). Then, the controller mode changes to fine search, in which the subcarrier frequencies are assigned by the fine search block (A4).

2) *Transmission through the Resonator*

The resonator acts as microwave filter. So, the output signal is attenuated corresponding to the transmission coefficient of the resonator. This means that if the resonator is excited at a subcarrier (see A2 and LO (1)) close to the resonance frequency, at the receiver (A3) we expect to receive a message with minimum Signal-to-Noise Ratio (SNR) compared to other subcarriers.

3) *Receiving the RF Signal and Post processing*

The received RF signal follows a similar route as the transmitted signal. In the SDR transceiver, LO (2) with the identical frequency to LO (1) down converts the signal and ADC converts the IF signal to discrete digital signals (Rx in Fig. 1). Finally, with digital down conversion and proper down sampling, the baseband signal is given back to the processing unit (A3).

On the processing unit, once the next message arrives at the input port (A3), the power of each sample of the vector will be calculated, integrated, and stacked in the buffer. When the buffer threshold exceeds, the minimum value of the buffer will be obtained and given to the fine search block.

In an iterative process, fine search block requests the controller to order the specific subcarrier frequencies. These frequencies are associated with the maximum attenuation of the filter. After meeting the user-defined criteria, the thread of processing unit will be completed, and the fine search frequency value will be interpreted as the real permittivity of the MUT.

III. Theoretical Foundation of the Proposed Procedure

As mentioned in Section II-C, we adopt a two-stage procedure to estimate the resonance frequency. The root of this procedure is in discrete Fourier transform (DFT)-based frequency estimation algorithms. This large group of estimators are utilized in estimation of complex single-tone discrete signals in two stages [40]. In the first stage (known as coarse search), a DFT is applied on the complex signal and the DFT bin with the maximum amplitude is selected. Then, in the fine search, the neighborhood of the selected DFT bin is explored until it converges to a local maximum. For global convergence of the algorithm, there should be only one peak within the selected neighborhood. However, considering the shape of the signal spectrum (i.e., a complex single tone), the algorithm converges to the global maximum even with small number of DFT bins [40].

The main difference between DFT-based algorithms is in their fine search method. Here, we employ AM algorithm [41], which is one of the simplest and most reputable DFT-based algorithms. In the fine search of this algorithm, selected DFT bin is recursively shifted until it converges to a local minimum. We modify AM algorithm (called as AM method) so it can be utilized in estimating the resonance frequency.

In addition to AM method, we utilize the Golden Section algorithm to find the optimal value of the fine search. Golden Section algorithm is a direct search, meaning it only requires validating the function itself, and information about higher derivatives (such as gradient) is not necessary. Starting at an initial bound, the Golden Section algorithm iteratively narrows down the bound while keeping the local minimum inside the bound. The algorithm stops when the neighborhood is lower than the user-defined tolerance.

In the following, coarse search and fine search as stages of the proposed procedure are discussed in detail.

A. Coarse Search

We assume the shift of resonance frequency f_r is limited to the bound of $[f_L, f_H]$ where $f_H - f_L = W$ is the total bandwidth. Our objective is to probe this bandwidth using a DFT-based coarse search. We divide the bandwidth W into N sections and excite N frequency points $(f_n; n = 0, \dots, N-1)$ at the beginning of each section. Instead of single carrier transmission, the proposed system is designed utilizing multicarrier topology.

This is due to complying with limited bandwidth of the SDR. Let us consider the passband signal with the form

$$s_P[k] = \sum_{n=0}^{N-1} Re\left(\zeta_k e^{j(\omega_c+\omega_n)k}\right);\ k = 0,1,\dots K-1, \quad (1)$$

where ζ_k is the $k-$th message sample, K is the total number of transmitted samples, $\omega_c = 2\pi f_c$, $f_c = (f_H + f_L)/2$, $\omega_n = 2\pi f_n$, and f_n is defined as

$$f_n = W\left(-\frac{1}{2}+\frac{n}{N}\right), \quad (2)$$

in which $f_c + f_n$ is associated with subcarrier frequency. The equivalent complex baseband signal can be written as

$$s[k] = \sum_{n=0}^{N-1} \zeta_k e^{j\omega_n k}. \quad (3)$$

We divide the observation window into N intervals each with $M \triangleq K/N$ samples. According to the proposed sensor system in Section II, the message associated with the $n-$th interval is

$$\zeta_k = \zeta\ \Pi\left(\frac{k}{M}-n\right) \quad (4)$$

where $\zeta \in \mathbb{R}$ is an arbitrary value and Π is the gate function defined as

$$\Pi(x) = \begin{cases} 1 & 0 \le x \le 1 \\ 0 & x < 0, 1 < x \end{cases}. \quad (5)$$

Substituting (4) in (3), the baseband signal $s[k]$ can be written as a summation over the intervals as

$$s[k] = \zeta \sum_{n=0}^{N-1} \Pi\left(\frac{k}{M}-n\right)\ e^{j\omega_n k}. \quad (6)$$

Then, the equivalent baseband signal at the receiver would be

$$\begin{aligned} r[k] &= (s * h)[k] + q[k] \\ &= \sum_{l=0}^{L} h[l,k]\, s[k-l] + q[k], \end{aligned} \quad (7)$$

where the symbol $*$ is linear convolution, $h[l]$ is the discrete impulse response of the resonator modeled as a complex filter with L non-zero taps, and $q[k] \sim CN(0,\sigma^2)$ is the additive white complex Gaussian noise with variance of σ^2. By substituting (6) into the equation (7), $r[k]$ can be written as

$$r[k] = \zeta \sum_{n=0}^{N-1}\sum_{l=0}^{L} h[l,k]\, \Pi\left(\frac{k-l}{M}-n\right) e^{j\omega_n(k-l)} + q[k], \quad (8)$$

Without loss of generality, we assume that for all the transmissions, the message is set to unity ($\zeta = 1$). By choosing a proper interval window (M) as $M \gg L$, the dependence of gate function on l can be neglected. So, we can simplify the equation (8) in the form of

$$r[k] = \sum_{n=0}^{N-1} \Pi\left(\frac{k}{M}-n\right) e^{j\omega_n k} \sum_{l=0}^{L} h[l,k]\, e^{-j\omega_n l} + q[k]. \quad (9)$$

For a specific value of m and n, we define the variable $y[m,\omega_n]$ as

$$y[m,\omega_n] \triangleq e^{j\omega_n m} \sum_{l=0}^{L} h[l,m]\, e^{-j\omega_n l} + q[m] \quad (10)$$

$$= x[m,\omega_n] \sum_{l=0}^{L} h[l,m]\, e^{-j\omega_n l} + q[m],$$

where $m = 0,1,\dots,M-1$ and

$$x[m,\omega_n] \triangleq e^{j\omega_n m}. \quad (11)$$

The summation can be seen as the discrete Fourier transform ($\mathcal{F}\{.\}$) of the filter at frequency ω_n as

$$\sum_{l=0}^{L} h[l,m]\, e^{-j\omega_n(l)} = \mathcal{F}\{h[l,m]\} = H(\omega_n, m). \quad (12)$$

Now by substituting equation (12) into (10) we can obtain the received signal $y[m,\omega_n]$ as

$$y[m,\omega_n] = x[m,n]H(\omega_n,m) + q[m]. \quad (13)$$

For the sake of simplicity, we suppose that the additive noise signal is negligible $q[m] \to 0$ (the case for high noise level is discussed in Appendix-I). Then, the power of the received signal is only a function of the resonator transfer function as

$$|y[m,\omega_n]|^2 = |x[m,\omega_n]H(\omega_n,m)|^2 = |H(\omega_n,m)|^2. \quad (14)$$

We assume that the resonator is a Notch filter with unit gain except for a neighborhood defined by parameters $\epsilon(\omega,m) \ll 1$ and δ in the form of [42]

$$|H(\omega,m)| = \begin{cases} 1 & |\omega-\omega_r(m)| > \delta(m) \\ \epsilon(\omega,m) & |\omega-\omega_r(m)| < \delta(m)' \end{cases} \quad (15)$$

where parameters $\epsilon(\omega,m)$ and $\delta(m)$ are related to the quality factor (Q-factor) of the Notch filter at the sample time m. Note that this assumption is reasonable since by coupling the SRR with microstrip line, a narrow stopband appears in the transmission coefficient of the resonator [30].

If we describe the received power in (14) using (15), then

$$|y[m,\omega_n]|^2 = \begin{cases} 1 & |\omega-\omega_r(m)| > \delta(m) \\ \epsilon^2(\omega,m) & |\omega-\omega_r(m)| < \delta(m) \end{cases}. \quad (16)$$

The aim is to obtain the interval $|\omega_n - \omega_r(m)| < \delta(m)$ and $\epsilon^2(\omega_n,m)$. In general, a frequency shifting resonator is a time-variant system, meaning that its responses to the identical inputs change with time. This is due to the changes of permittivity of the MUT in time. Nevertheless, we assume during the sensing cycle, characteristics of the MUT are consistent. With this relaxation, we can approximate the system as time-invariant. So, we drop the dependence of the resonator transfer function in (16) on sample time (m), which results in

$$|y[m,\omega_n]|^2 = \begin{cases} 1 & |\omega-\omega_r| > \delta \\ \epsilon^2(\omega) & |\omega-\omega_r| < \delta \end{cases}, \quad (17)$$

yielding that for the whole transmission time slot (n), the resonator's response is independent from individual samples (m). Thus, we use a discrete-time integrator to accumulate the transmitted power as

$$|y[\omega_n]|^2 = \frac{1}{N}\sum_{m=0}^{M-1} |y[m,\omega_n]|^2 = \begin{cases} 1 & |\omega-\omega_r| > \delta \\ \epsilon^2(\omega) & |\omega-\omega_r| < \delta \end{cases}. \quad (18)$$

These values are sequentially stored in the buffer until the threshold exceeds. Considering the buffer size (N), the whole process takes $K = M \times N$ samples. Then, the output of the buffer would be a combination of different return powers each for a specific frequency as

 Published version: https://doi.org/10.1109/JSEN.2022.3225662

$$\mathbf{y} = \{|y[\omega_n]|^2 \mid n = 0, \dots, N-1\}. \quad (19)$$

Considering (18), with a proper choice of N, the minimum value of this vector lies within the neighborhood of $|\omega_n - \omega_r| < \delta$. So that

$$\min_{\omega_n} \mathbf{y} = (\epsilon^*)^2 = \epsilon^2(\omega_{n^*}), \quad (20)$$

with ω_{n^*} being as the optimal value of the coarse search.

B. Fine Search

The optimal value of the coarse search (ω_{n^*}) approaches to the global value ($\omega^* = 2\pi f_r$) when $N \to \infty$. However, this is impractical as the number of samples increases with $O(N)$, resulting in longer transmission time, which takes undesirably much longer time for each experiment (i.e., sensing cycle) to finish. Moreover, reaching higher resolutions for a large bandwidth requires high quality components which can result in expensive solutions.

To address this issue, we employ fine search strategies, in which the resolution improves in a recursive manner. We assume that the global minimum of the function $|H(\omega)|$ lies in the neighborhood of $|\omega_{n^*} - \omega_r| < \delta$ (selected neighborhood), where within this range $|H(\omega)| = \epsilon(\omega)$ is a convex function. The Euclidian distance between the resonance frequency ω_r and the output of the coarse search ω_{n^*} is defined as $\delta^* = \omega_{n^*} - \omega_r$. The main goal of the fine search is to estimate the residual frequency δ^* which leads to ω_r, the argument of the minima. In addition, we consider that ω_{n^*+1} and ω_{n^*-1} also lie within the range of the selected neighborhood, where

$$\omega_{n^*-1} = \omega_{n^*} - 2\pi\frac{W}{N}\ ;\ \omega_{n^*+1} = \omega_{n^*} + 2\pi\frac{W}{N} \quad (21)$$

so that $|\omega_{n^*+1} - \omega_r| < \delta$ and $|\omega_{n^*-1} - \omega_r| < \delta$. This can be realized using proper choice of N.

We developed two recursive methods inspired by AM algorithm [41] and Golden-Section optimization algorithm [43], respectively. In both methods, the goal is to find δ^* (the shift between coarse search optimal value ω_{n^*} and the actual resonance frequency ω_r).

1) *AM method*

At each stage (i −th) of this method, the frequency ω_{n^*} will be shifted until the residual $\delta_i \to \delta^*$. Starting with initial conditions ($i = 0$), we excite the resonator at frequencies of

$$\omega_{(n^*\pm p, i=0)} = \omega_{n^*} + 2\pi(\delta_{i=0} \pm p)\frac{W}{N};\ \ p = \frac{1}{2}, \quad (22)$$

where $\omega_{(n^*,i)}$ is the shifted frequency at stage (i) and $\delta_0 = 0$. To update $\delta_i, for\ i = 1, \dots$, we utilize the following update algorithm [41]

$$\delta_i = \delta_{i-1} + h(\delta_{i-1}), \quad (23)$$

where $h(\delta_{i-1})$ is defined as [41]

$$h(\delta_{i-1}) = -\frac{1}{2}\frac{|y[\omega_{(n^*+p,i-1)}]| - |y[\omega_{(n^*-p,i-1)}]|}{|y[\omega_{(n^*+p,i-1)}]| + |y[\omega_{(n^*-p,i-1)}]|}. \quad (24)$$

We substitute δ_i from (23) and (24) into equation (22) to update the exciting frequencies $\omega_{(n^*\pm p,i)}$ as

$$\omega_{(n^*\pm p,i+1)} = \omega_{n^*} + 2\pi(\delta_{i=0} \pm p)\frac{W}{N} \quad (25)$$

This process will continue until $h(\delta_{i-1}) < tol$, where tol is a user defined variable.

2) *Golden-Section method*

At i −th stage of the method, the range is described as

$$\Delta(i) = b(i) - a(i), \quad (26)$$

where $b(i)$ and $a(i)$ are the upper and lower limits, respectively. The procedure of narrowing down the range $\mathrm{d}(i)$ starts by introducing two potential points defined as [43]

$$\begin{aligned} c(i) &= b(i) - \Delta(i)/\mathrm{gr}\,, \\ d(i) &= a(i) + \Delta(i)/\mathrm{gr}\,, \end{aligned} \quad (27)$$

where gr is a ratio to control the length of each step. In the optimal setting, it is given by

$$\mathrm{gr} = \frac{\sqrt{5}+1}{2}, \quad (28)$$

known as the golden ratio.

At the initial conditions ($i = 0$), we define $b(0) = \omega_{n^*+1}$, and $a(0) = \omega_{n^*-1}$, respectively, and we excite the resonator in two frequencies of $c(0)$ and $d(0)$ which are

$$\begin{aligned} c(0) &= b(0) - \Delta(0)/\mathrm{gr}, \\ d(0) &= a(0) + \Delta(0)/\mathrm{gr}, \end{aligned} \quad (29)$$

with $|y[c(0)]|$ and $|y[d(0)]|$ as the corresponding outputs from the resonator. Golden-Section is a conditional algorithm, so based on a comparison between these outputs, the next step will be chosen. Specifically, at the stage ($i; i \geq 0$), we have the following conditions [43]

$$\begin{cases} b(i+1) = d(i) \\ a(i+1) = a(i) \end{cases} \quad |y[c(i)]| < |y[d(i)]| \\ \begin{cases} b(i+1) = b(i) \\ a(i+1) = c(i) \end{cases} \quad |y[c(i)]| \geq |y[d(i)]| \quad (30)$$

The iterative procedure redefines the range (26) for $i + 1$ using (30). The stop criterion is met when ($\Delta(i+1) < tol$), where tol is a user defined variable.

IV. Sensor System Implementation

In this section, we implement a prototype of the proposed sensor system. Specifically, we employ a processing unit and an SDR transceiver for the sensor data measuring device. In addition, for the sensor we fabricated one of the existing resonator designs. All the configurations of the prototype are aligned with the setting of Section II. The details are as follows.

A. The Processing Unit

For the processing unit, we use a central processing unit (CPU) machine. The CPU machine is a laptop with CPU of Intel Core-i7 and 16 Gigabytes of RAM running GNU Radio software on Linux Ubuntu operating system. It is worth mentioning that considering the ports of SDR system, an FPGA or a microcontroller can also handle the operations.

For the message (A1) we utilize $M = 512$ samples of a complex single tone signal with the normalized frequency of $2\pi/8$. We select $f_L = 2GHz$ and $f_H = 3GHz$ as the lower and upper bound of the resonator's bandwidth ($W = 1GHz$). The message is transmitted via $N = 50$ subcarriers, each with corresponding frequency $f_c + f_n$. The transmission of message on a specific subcarrier takes up to $4M$ samples, thus we choose the delay τ as $5M$ samples. To find the minimum value of the buffer, we used Linear Search algorithm.

In the fine search, we explore the neighborhood of ω_{n^*} using either AM method or Golden-Section method. In Golden

Published version: https://doi.org/10.1109/JSEN.2022.3225662

Section, the search stops when the bound is lower than the user defined tolerance ($tol = 10KHz$) or its corresponding number of iterations. AM method either converges to $tol = -30dBm$ or reaches to a maximum number limit iteration $iter_{max} = 10$. On average, AM method reaches its optimal value on $N_{AM} = 4$ iterations and $2 \times N_{AM} \times M$ samples are efficiently transmitted. The Golden-Section reaches the optimal value on $N_{GS} = \lceil \ln(tol/W)/\ln(1 - 1/gr) \rceil = 8$ and $N_{GS} \times M$ samples are efficiently transmitted.

B. SDR Configuration

For the sensor system, any general SDR supported by GNU Radio can be utilized. Here, we employed a National Instrument Universal Software Radio Peripheral (USRP) B200 mini. The RF coverage of this device is from 70 MHz to 6 GHz, with 56 MHz bandwidth and 61.44 Msps sampling frequency.

We connect the SDR to the resonator using SMA cables. The RF front end of the USRP consists of an Analog Devices AD9364 transceiver with 12-bits ADC/DAC. To handle baseband discrete signals, the transceiver is connected to a Xilinx Spartan-6 FPGA. Finally, we communicate with the USRP (FPGA port) via a Universal Serial Bus (USB) version 3. The overall settings of the SDR are given in Table-I.

C. Resonator sensor design

The sensitivity as well as the working frequency of the SRR depend on different parameters such as number of rings, the gap between split rings, the width of rings, and the distance between them [44]. In addition, the shape of the rings (square, circular, etc.) creates different equivalent circuits, which is suitable for different applications. Some designs suggest employing more advanced designs to achieve higher sensitivity (for instance [2] and [11]). However, in principle the scattering parameters of such resonators can be modeled as a Notch filter. Here, the sensor design is taken from [45], which has a planar structure composed of two rectangular rings fed by a microstrip transmission line. The design is chosen based on low-complexity fabrication, and the ability of the resonator to recognize changes in solids and liquids characterizations as well as material thickness [45].

The resonator is implemented on an FR-4 (glass-reinforced epoxy) substrate sheet with thickness of $h = 1.5\ mm$. Moreover, the metallization thickness, dielectric constant and loss tangent of this material are $35\ \mu m$, $\varepsilon_r' = 4.4$ and $\tan\delta = 0.02$, respectively.

The physical layout of the resonator is shown in Fig. 2. In this design, two identical spilt rings are coupled to the microstrip line. Each one of these split rings are resonators, in which the resonance frequency is mainly a function of dimension of the external ring and the gap between split rings. To guarantee that the radiation boundaries of the resonator are defined within the boundaries of the MUT, the length of microstrip lines in the y-axis is extended, that is, the submersible resonator would be roughly in the middle of the MUT.

TABLE I
SDR CONFIGURATION SETUP

Configuration	Value
SDR transmission bandwidth	$1KHz$
Starting frequency (f_L)	$2GHz$
Stop frequency (f_H)	$3GHz$
Digital Up conversion Rate	$64\ KSps$
Transmitted Power (dBm)	$-15\ dBm$
Local oscillator offset (LO_{offset})	$0\ Hz$

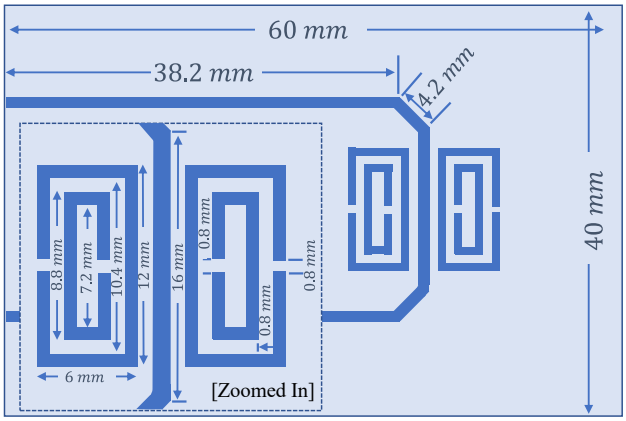

Fig. 2. Physical Layout of the resonator based on [45]. For better visibility, the split rings are enlarged in the image.

When both SRRs experience the same boundary (the same medium), the depth of transmission coefficients (S_{12}/S_{21}) at the resonance frequency will be amplified.

D. Simulation of the Resonator

As shown in Fig. 3, we implement the resonator in Ansys High Frequency Simulation Software (HFSS). For all the simulations, we utilized adaptive mesh refinement with initial value of three elements per wavelength and lumped port excitation with 50-ohm impendence. The selected boundary for simulation is a cube filled with air with the size of (70 mm, 50 mm, 12 mm) in the Cartesian coordinate system. We place the resonator at the center of boundary. Moreover, for the materials, we assume FR-4 and copper for the substrate and surface of the layout, respectively.

The isolation s-parameter, S_{12} , of the resonator is illustrated in Fig. 4 showing a Notch at the frequency of $f_r = 2.56$ GHz, with the depth of -11.26 dB, which is the resonance frequency of resonator.

Also, to study the concentration of electric field (E-field) at the resonance frequency (f_r), we simulate the E-field distribution on the surface of the resonator at two different frequencies, namely 2 GHz and 2.56 GHz (ω_r), shown in Fig. 5 (a) and (b), respectively. As it is apparent in Fig. 5 (a), when the resonator is excited with a frequency other than the resonance frequency, the electric field is distributed along the microstrip

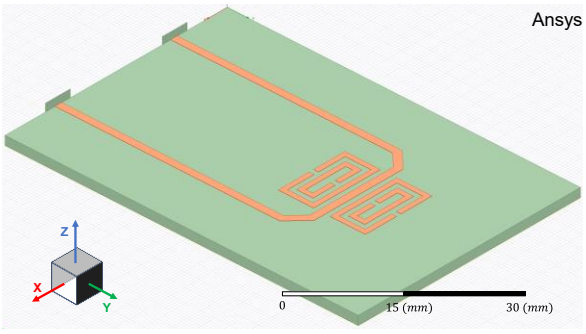

Fig. 3. Resonator Model in Ansys HFSS. In this figure, green and orange materials are FR-4 and copper, respectively.

Published version: https://doi.org/10.1109/JSEN.2022.3225662

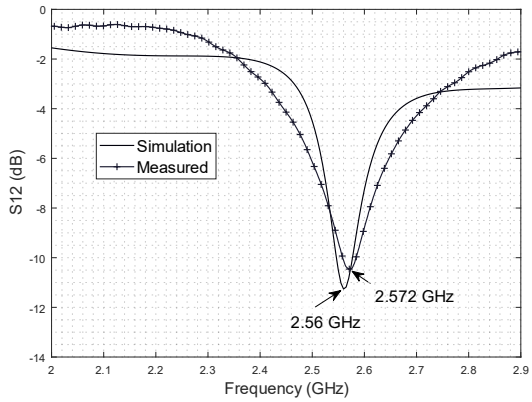

Fig. 4. Dependency of S_{12} of the resonator on Frequency for simulation and measured data. Arrows indicate the frequency associated with the deep Notch of the resonator for each plot

transmission line. However, at frequency 2.56 GHz, the field is concentrated around the spilt rings.

E. Equivalent Circuit

SRR equivalent circuits can be modeled as an LC Notch filter with the resonance frequency of

$$f_r = \frac{1}{2\pi}\frac{1}{\sqrt{L_r C_r}} \tag{31}$$

where the total capacitance C_r is related to the gap between the rings, whereas the inductance L_r is a function of perimeter of the external ring [45]. Noting that in a more accurate model, the influence of mitered bends in the microstrip line can also be incorporated as inductance and capacitance into the circuit.

F. Sensing Principle

As it is illustrated in Figure 5 (b), when the resonator is excited at the resonance frequency f_r, the electric fields are dispersed between the conductor and ground plane of the split rings. For this case, the effective permittivity is defined as [45]

$$\varepsilon_{eff} = \frac{\varepsilon_r+1}{2} + \frac{\varepsilon_r-1}{2}\left(\frac{1}{\sqrt{1+12h/c}} + 0.04(1-h/c)^2\right), \tag{32}$$

where ε_r is the relative permittivity of the medium (air as default) covered the microstrip conductor and based on the physical layout shown in Fig. 2, and the width of microstrip line is $c = 0.8\,mm$. For this specific design, we can write ε_{eff} in equation (36) as a linear function of relative permittivity as

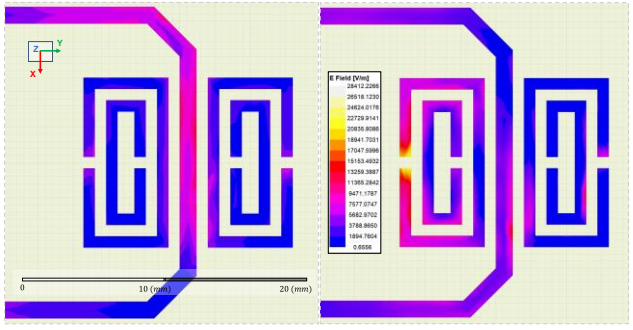

(a) (b)

Fig. 5. Electric Field on the surface of the resonator for (a) 2 GHz and (b) 2.56 GHz (resonance frequency). In the resonance frequency, the electric field is concentrated around the spilt rings

$$\begin{gathered}\varepsilon_{eff} = \alpha\varepsilon_r + \beta,\\ \alpha \triangleq \frac{1}{2} + \frac{1}{2}\left(\frac{1}{\sqrt{1+\frac{12h}{c}}} + 0.04\left(1-\frac{h}{c}\right)^2\right) = 0.6185,\\ \beta \triangleq \frac{1}{2} - \frac{1}{2}\left(\frac{1}{\sqrt{1+\frac{12h}{c}}} + 0.04\left(1-\frac{h}{c}\right)^2\right) = 0.3815.\end{gathered} \tag{33}$$

There is a direct relationship between capacitance and inductance of resonator (equation (31)) and the squared root of effective permittivity [45]. This way, the resonance frequency is also a function of effective permittivity as

$$f_r = \frac{1}{2\pi}\frac{1}{\sqrt{\varepsilon_{eff}}}\gamma\,. \tag{34}$$

where γ is related to the physical shape of the resonator. Assume the medium containing the sensor experiences a change of state (from state $0 \to 1$). This results in changing the relative permittivity as

$$\varepsilon_r(1) = \varepsilon_r(0) + \Delta\varepsilon_r, \tag{35}$$

where $\varepsilon_r(0)$ and $\varepsilon_r(1)$ are the relative permittivity of state zero and one, respectively. Then the $\varepsilon_{eff}(1)$ (effective permittivity at state 1) will be written as

$$\begin{gathered}\varepsilon_{eff}(1) = \alpha\varepsilon_r(1) + \beta\\ \varepsilon_{eff}(1) = \alpha(\varepsilon_r(0) + \Delta\varepsilon_r) + \beta\\ \varepsilon_{eff}(1) = \varepsilon_{eff}(0) + \alpha\Delta\varepsilon_r,\end{gathered} \tag{36}$$

where $\varepsilon_{eff}(0)$ is the effective permittivity of state zero. By incorporating these changes into the equation (34), we can describe the effect of change in the relative permittivity of resonance frequency as

$$\omega_r(1) = \frac{1}{\sqrt{\varepsilon_{eff}(1)}}\gamma = \frac{1}{\sqrt{\varepsilon_{eff}(0) + \alpha\Delta\varepsilon_r}}\gamma, \tag{37}$$

which can be approximated using Taylor series expansion as

$$\begin{gathered}\omega_r(1) \cong \frac{1}{\sqrt{\varepsilon_{eff}(0)}}\gamma - \frac{1/2\alpha}{\sqrt{\varepsilon_{eff}^3(0)}}\Delta\varepsilon_r\gamma\\ \omega_r(1) \cong \omega_r(0) - \frac{\frac{1}{2\alpha}}{\sqrt{\varepsilon_{eff}^3(0)}}\Delta\varepsilon_r\gamma.\end{gathered} \tag{38}$$

Finally, the change in the relative permittivity can be described in terms of resonance frequency as

$$\begin{gathered}\Delta\varepsilon_r = s_r\left(\omega_r(0) - \omega_r(1)\right)\\ s_r \triangleq \frac{2\alpha\sqrt{\varepsilon_{eff}^3(0)}}{\gamma}\end{gathered} \tag{39}$$

G. Fabrication

To fabricate the resonator, first, we export the Drawing Exchange Format (DXF) files of the HFSS design into Multisim Ultiboard Software to get Gerber files of the Printed Circuit Board (PCB) layout. Then we utilize an LPKF® Protomat S63 PCB prototyping device to drill the design on a sheet of FR-4 epoxy with both parts covered by copper. Finally, two male SubMiniature version A (SMA) type connector is soldered at each port. The measured isolation s-parameter, S_{12} of the fabricated resonator is shown in Fig. 4 which is in agreement with the simulations.

Published version: https://doi.org/10.1109/JSEN.2022.3225662

V. Simulations and Experiments

In this section we conducted simulations and measurements for validating the performance of the proposed sensor system. In the simulation environment (MATLAB software), we estimate the resonance frequency of a complex notch filter using the theoretical foundation of the proposed procedure (Section III). We investigate the estimation performance in terms of DFT resolution, observation time and filter bandwidth. Moreover, we created an experiment setup, where we can compare the performance of the prototyped sensor system (Section IV) against state-of-the-art measurement equipment.

A. Simulations

In the simulations, we assume an equivalent model of the proposed sensor system, which helps us generalize the performance evaluations. Specifically, for the resonator we utilize a complex Notch filter with the transfer function of [46]

$$H_{sim}(z) = \frac{1 - e^{j\omega_r} z^{-1}}{1 - \rho e^{j\omega_r} z^{-1}}, \tag{40}$$

in which $\omega_r \in (-\pi, \pi)$ is the resonance frequency and parameter $\rho \in (0,1)$ controls the bandwidth of the Notch filter. The parameter ρ can be fitted as a quadratic function of 3 dB-bandwidth (W_r) in the form of

$$\rho = -0.135{\mathrm{W}_r}^2 - 0.5\mathrm{W}_r + 1, \tag{41}$$

with R-squared $R^2 \cong 1$. In addition, we assume the filter is excited using the equivalent baseband signal defined in (6), where $\zeta = 1$ and $W = [-0.5, 0.5]$.

Subsequently, the output of the Notch filter for $\mathrm{m}-\mathrm{th}$ sample of subcarrier ω_n can be described as

$$y[m, \omega_n] = (x * h_{sim})[m, \omega_n] + q[m, \omega_n]. \tag{42}$$

where h_{sim} is the impulse response of $H_{sim}(z)$ in time domain and $q[m, \omega_n]$ is defined based on (10) with a variance of $\sigma^2 = 10^{-SNR/10}$, where SNR is the signal-to-noise ratio in decibel.

To study the principle behind the coarse search of the proposed procedure (Section III-A), the periodogram ($|Y(\omega_n)|^2$) of the output vector $\boldsymbol{y}[\omega_n]$ is calculated. The vector $\boldsymbol{y}[\omega_n]$ is defined as

$$\boldsymbol{y}[\omega_n] = \{y[0, \omega_n], y[2, \omega_n], \dots, y[M-1, \omega_n]\}. \tag{43}$$

The results of this simulation are shown in Fig. 6 (a). We set $N = 64$ and $M = 1024$ for the equivalent signal in (6), while the resonance frequency and bandwidth of the filter are chosen as $\omega_r = -0.4\pi$ and $\mathrm{W}_\mathrm{r} = 0.1\pi$ respectively. In this figure, x-axis shows the subcarrier frequencies and y-axis is related to the frequency bins associated with received signal periodogram.
As it is noted in the color bar, pixels with lighter colors hold higher values of $|Y(\omega_n)|^2$. As expected, the frequency bins in which the $|Y(\omega_n)|^2$ is maximum, are associated with the corresponding subcarrier f_n (anti-diagonal white pixels). However, there is a lack of received power in the neighborhood of $\omega_r - \mathrm{W}_r/2 \le \omega_n \le \omega_r + \mathrm{W}_r/2$.

Next, for each value of parameter n (each column of Fig. 6 (a)), the received power samples ($m = 0, \dots, M-1$) go through a discrete-time integrator. The outputs of this block ($\left|y[\omega_{(.)}]\right|^2$) only depend on the parameter n and its associated frequency (see (18)). It is shown in Fig. 6 (b) that the output values follow the same shape as the filter spectrum ($|H_{sim}(j\omega)|^2$), which supports the theory found in equation (17). In fact, this feature helps us to obtain a local minimum in the coarse search, which for this example is $n^* = 19$ corresponding to $\omega_{n^*} = -0.3968\pi$, with residual value of $\delta = |\omega_r - \omega_{n^*}| = 0.0032\pi$ lower than W_r.

In the following simulations, we use the mean squared error (MSE) as the measure to validate the quality of frequency estimations. The MSE can be defined as

$$\mathrm{MSE} = \frac{1}{MC}\sum_{i=1}^{MC}(\omega_r - \widehat{\omega})^2, \tag{44}$$

where MC is the number of Monte Carlo simulations and $\widehat{\omega}$ is the estimated frequency.

First, we examine the performance of estimation merely based on coarse search. We set $MC = 1000$, $SNR = 10\,dB$. We also assume the filter has a bandwidth of $\mathrm{W}_\mathrm{r} = 0.1\pi$ while for each Monte Carlo simulation, the resonance frequency is chosen from the uniform distribution $\omega_r \sim U(-\pi, \pi)$.
The influence of parameters M and N on the accuracy of coarse search is investigated in Fig. 7. We observe that the parameter N, which can be interpreted as the DFT resolution, is the limiting factor of MSE. In fact, for a specific value of N the increase in the observation time (M), can only reduce the MSE to some certain extent and then, the MSE will proceed to a lower limit.

In Fig. 8, we investigate this limiting factor on the fine search methods. In details, we select a specific value of $N = 128$ and then we obtain the dependence of MSE on the observation length (M) for AM method and Golden Section method, both with 5 and 10 iterations. Employing fine search methods, the final estimate is improved up to ten times solely based on increasing the value of M. Note that to obtain this accuracy (10^{-4} MSE), coarse search estimate requires the resolution of $N = 1024$ DFT bins (see Fig. 7). In comparison between AM method and Golden Section method, we observe that AM method achieves better results, which supports the fact that with

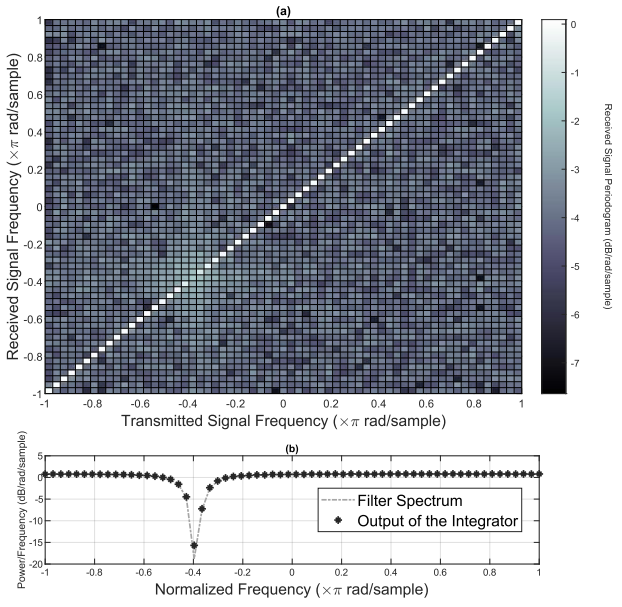

Fig. 6. (a) Dependency of received signal periodogram on transmitted single tone for different frequencies. The periodogram experiences up to −3 dB reduction in power when $\omega_r - \mathrm{W}_r/2 \le \omega_n \le \omega_r + \mathrm{W}_r/2$. (b) Dependency of output of the integrator on the frequency of transmitted single tone. The output values follow the same pattern as the filter spectrum.

Published version: https://doi.org/10.1109/JSEN.2022.3225662

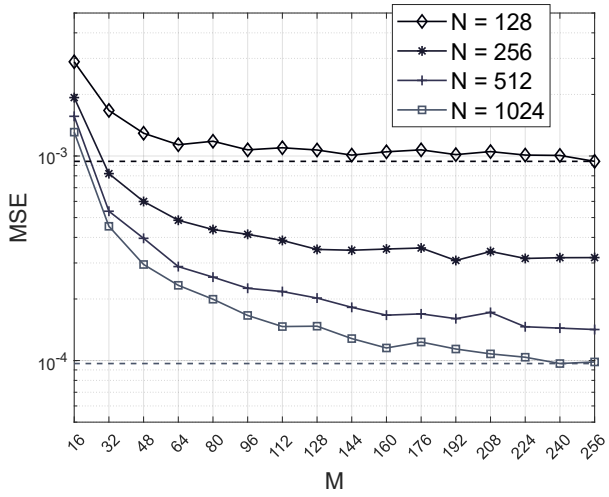

Fig. 7. Dependency of MSE of coarse search estimation on parameters M and N. For a fixed N, as the parameter M increases the MSE of frequency estimation will reach to a lower limit.

a symmetrical transfer function, AM performs better than Golden Section.

Finally, the dependence of MSE on the bandwidth W_r is shown in Fig. 9. For this simulation, we set $N = 128$ and $M = 256$, and SNR $= 10\,dB$. It can be observed that when the bandwidth of the filter increases, the MSE of fine search methods approaches to the MSE of coarse search. In fact, fine search methods rely on the sharpness of stopband at the resonance frequency, which has inverse relationship with the bandwidth W_r. This is the limitation of proposed procedure, indicating that for filters with normalized bandwidths larger than 0.2π, the gain of fine search methods is limited.

B. Experiments

The results of Section IV-E and Fig. 5 (b) give us the intuition to place the MUT on the surface and close to the resonator. The same as [45], we immerse the sensor into the liquid. For the container, we use a glass with the shape of frustum cone. In this frustum, radius of the smaller circle and radius of bigger circle are 21 mm and 29.2 mm, respectively. We fill the container with

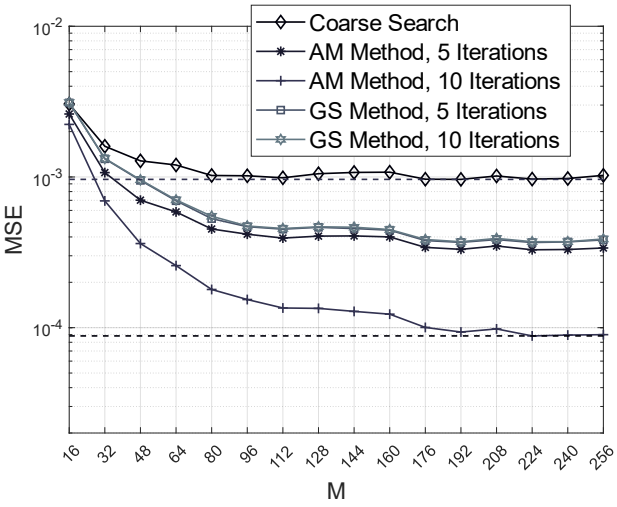

Fig. 8. Dependency of MSE on parameter M for fixed $N = 128$ and different estimators. Using AM method, an accuracy 10 times higher than the original coarse search is achievable.

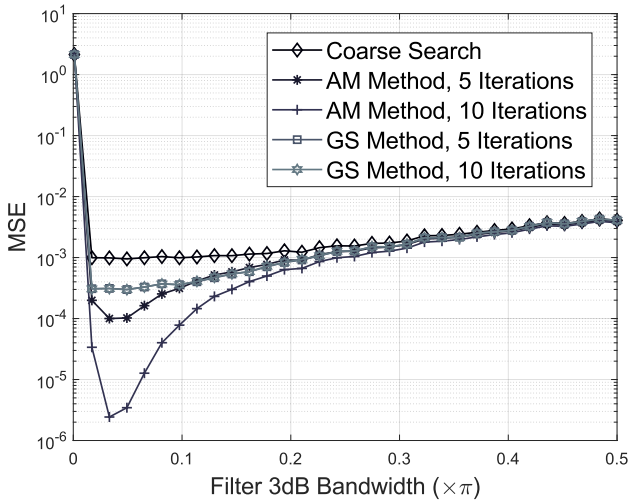

Fig. 9. Dependency of MSE the bandwidth of filter (W_r). Performance of the fine search estimators degrades when bandwidth increases, which is the limitation of proposed approach.

68 mL of MUT, which is about 34 mm height of the glass. To keep the sensor in place, we tape it from the SMA ports to the glass. The measurement setup is shown in Fig. 10. All the measurements are done in the room temperature (27 degrees Celsius).

For the liquid in the container, the solution of distilled water and Methanol is utilized. To keep the height of liquid at the same level, at each step we remove 5 mL of the solution (consisting of both water and Methanol) then 5 mL of solute (either water or Methanol) will be added. Note that this is important as changing the height of the container will change the contacting surface of the microstrip conductor.

Initially, the container is filled up with 68 mL of 100 percent distilled water. Next, we connect the SMA connectors of resonator to SDR system using a Female SMA to Female SMA coaxial cable with 1.5m long.

Proposed sensor system estimates the resonance frequency of the resonator and corresponding permittivity of MUT using the setup in Section IV.

For the sake of comparison, we perform the same experiment within a short time window by a VNA. To do so, we disconnect the cable from the SDR's end, and then connect it to the VNA. The VNA utilized here is an R&S®ZNB 8, with 1857 points frequency sweep within the range of (2 GHz, 3 GHz) (distance between two consecutive points approximately 538 KHz). For this specific VNA, synthesizing each point takes around 1 μ.

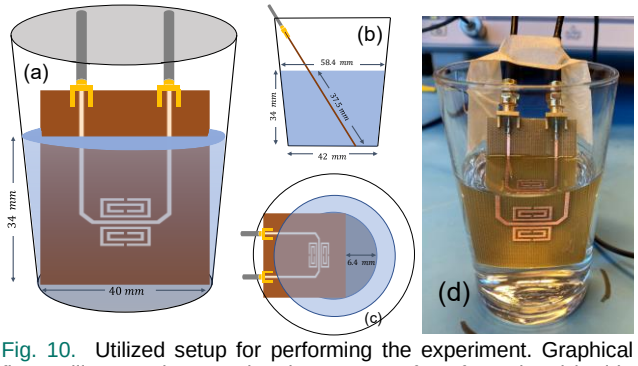

Fig. 10. Utilized setup for performing the experiment. Graphical figures illustrate the associated parameters from front view (a), side view (b) and above (c). The final setup is shown in the picture (d).

Published version: https://doi.org/10.1109/JSEN.2022.3225662

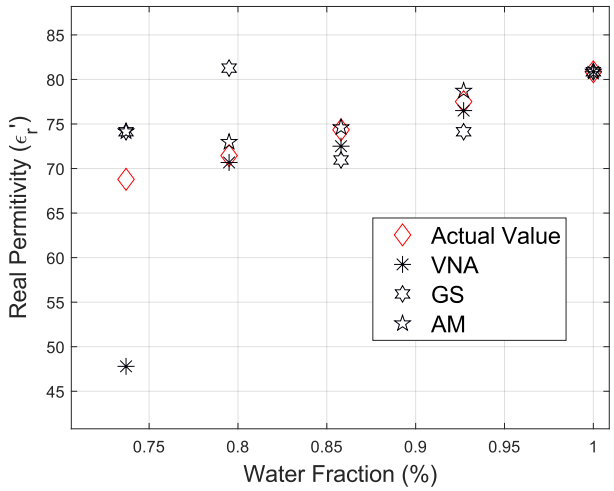

Fig. 11. The comparison between measured data with VNA and SDR (AM method and Golden Section method) to realize the dependency of real permittivity on water fraction. There is a good agreement between measured data and theory up to 20 percent Methanol.

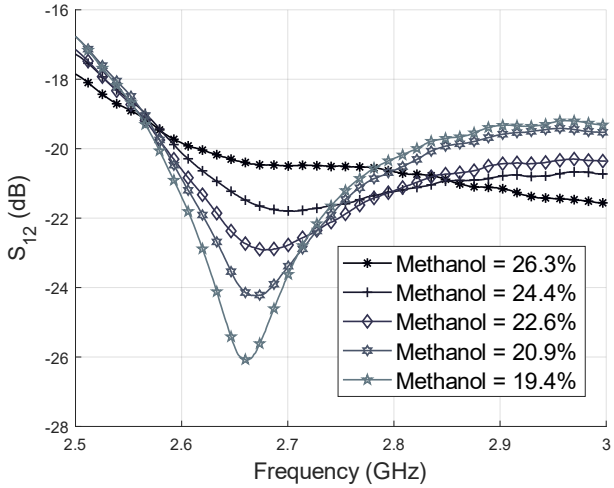

Fig. 12. Dependency of measured transmission response (S_{12}) of the resonator for methanol-water experiments. The resonator fails to provide a sharp Notch when the methanol contribution increases higher than 20 percent.

Note that to obtain the real permittivity of the MUT using the VNA, we make use of the manual frequency sweep to find the minimum of S_{12}. Then we extract the data using a USB flash drive and import it into the MATLAB software. Further, in offline post processing, we apply linear regression to obtain the variation in the value of permittivity characteristic of the MUT.

Now we repeat the whole step four times but with different percentages of solute. We remove 5 mL from the solution and add 5 mL of Methanol (impurity less than 10 ppm). This creates a solution with 7.3%, 14.2%, 20.5%, and 26.3% of Methanol as the solute. At each step, we carry out the measurements identical to the initial step (with both SDR and VNA).

The measured resonance frequencies for all the experiments are shown in Table II. The table consists of frequencies in which S_{12} reaches to its minimum value. Moreover, to investigate the performance of each algorithm in details, the absolute difference between VNA and both proposed procedures are calculated. It can be observed that for up to 20 percent Methanol, Golden Section method accurately follows the pattern of exhaustive search values. However, for higher percentages it diverges from the actual value. In addition, AM method can only follow the increase in the frequency domain, not the actual sharpness. In fact, as it is discussed in Section III-B, the method converges to the optimal value only if the function $\epsilon(\omega)$ is symmetric. Thus, any asymmetry in the objective function leads to a bias on the local minimum estimation.

Next, to estimate the real permittivity of the water-methanol solution, we fit the measured frequencies of each method to (39), which results $s_r = 1.083 \times 10^{-8}$, $s_r = 1.28 \times 10^{-8}$, and $s_r = 7.785 \times 10^{-8}$ for VNA exhaustive search, Golden section method and AM method, respectively. For the ground truth of real permittivity, we used the data for binary mixture of methanol and water reported in [38]. It is worth mentioning that after sensor system calibration and extracting the linear regression coefficients, the whole process can be accomplished in an online manner.

The results are given in Fig.11, showing an agreement between the experiments and theoretical values up to 20 percent Methanol (like findings of Table II). However, it is apparent that with slope adjustment of the AM method can describe the permittivity based on water fraction, better than Golden section method.

To explain why the measurements diverge from the theoretical values for methanol fraction higher than 20 percent, we perform five more experiments with 26.3%, 24.4%, 22.6%, 20.9%, and 19.4% methanol concentration, respectively. In these experiments, we keep all the data points from the VNA, which are shown in Fig. 12. Apparently, the depth of the resonance frequency substantially degrades when the contribution of Methanol increases. This is indeed with agreement of resonator Q-factor definition. In this situation, the coarse search fails to find the proper neighborhood and subsequently gets stuck in a local minimum.

TABLE II
MEASURED FREQUENCIES USING EXHAUSTIVE SEARCH ON VNA AND AM METHOD AND GOLDEN SECTION METHOD ON SDR

Methanol Percentage	Frequency associates with minimum value of S_{12}			Absolute Difference	
	VNA Device	Golden Section	AM Algorithm	VNA and Golden Section	VNA and AM
0%	2.511409 GHz	2.510995 GHz	2.549451 GHz	4 KHz	38.04 MHz
7.3%	2.575431 GHz	2.605995 GHz	2.553831 GHz	30.56 MHz	21.6 MHz
14.2%	2.634159 GHz	2.650686 GHz	2.562218 GHz	16.52 MHz	71.94 MHz
20.5%	2.661004 GHz	2.505186 GHz	2.565583 GHz	155.81 MHz	95.42 MHz
26.3%	2.997306 GHz	2.605971 GHz	2.563152 GHz	78.83 MHz	121.65 MHz

Finally, in Table III the proposed microwave sensor system is compared in terms of working frequency and relative error of the real permittivity (ϵ') with the state-of-the-art sensors. The relative error is defined as

$$Relative\ Error = \frac{\left|\epsilon'_{actual\ value} - \epsilon'_{measured}\right|}{\epsilon'_{actual\ value}} \times 100 \qquad (45)$$

For the proposed sensor system, we consider the measurements with VNA, and with SDR when AM method and Golden Section method are applied. In [2], a stepped impedance resonator (SIR) is used for methanol and ethanol permittivity characterization. In [35] the sensor uses CSRR as the sensing node as well as VNA and SDR as the measuring instruments. The sensor in [22] uses a differential SRR (DSRR) in addition to VNA for measurements, while in [33] an alternative circuit design based on injection-locked oscillator (ILO) is developed. Based on the provided details in Table III, the performance of sensor system degrades (up to 6.01 % for [35]), when VNA is substituted with SDR and alternative circuits. Nevertheless, with employing the frequency estimation approach in the proposed sensor system, the decline on the performance is well-compensated (0.26 % and 3.07 % for AM method and Golden Section method, respectively). Moreover, for identical MUTs the proposed sensor surpasses the state-of-the-art counterparts, regardless of the measuring device.

VI. Conclusions

Our main objective was to provide a low-cost and accurate microwave sensor system, which can be used as a reliable and a general measuring device for estimating real permittivity characteristic of the MUT in the testing stage and laboratory setting. We assumed the sensor is a resonator with shifting resonance frequency and any shift in the resonance frequency of the resonator is caused by changes in the MUT permittivity.

Knowing that the existing solutions in the literature are either designed for specific applications (alternative circuit designs) or high-priced (e.g., VNA and AWG), we develop a simple yet efficient sensor system to detect the changes in the real part of relative permittivity of the MUT. The proposed system can be implemented using any general SDR transceiver supported by GNU Radio. In addition, due to the simplicity of calculations, simple processing unit can be employed to estimate the frequency shift. Owing the flexible structure of the system, working frequency, bandwidth, number of subcarriers, and observation time can be reconfigured to the requirement of applications. In addition, the proposed frequency estimation methods can be easily updated and replaced with other methods. Consequently, the user can test different resonator designs without any challenge on the sensor system modification.

TABLE III
Comparison Between Various Microwave Sensor Systems

Sensor System	Frequency	MUT	ϵ' Relative Error
SRR w/VNA	2.56 GHz	Methanol (%7)	1.29 %
SRR w/SDR + AM	2.56 GHz	Methanol (%7)	1.55 %
SRR w/SDR + GS	2.56 GHz	Methanol (%7)	4.36 %
SIR w/VNA [2]	1.91 GHz	Methanol	4.5 %
CSRR w/VNA [35]	1.25 GHz	RT/duroid 5870	1.71 %
CSRR w/SDR [35]	1.25 GHz	RT/duroid 5870	7.72 %
DSRR w/VNA [22]	1.9 GHz	RT/duroid 5880	3.6 %
ILO-based [33]	1 GHz	RT/duroid 6010	3.3 %

The proposed sensor system substitutes the exhaustive search with a smarter strategy. Thus, it can significantly improve the estimation accuracy within the same observation time and resolution. We find this property desirable for the low-cost applications with limited resolution and rapidly changing environment in which the permittivity value might be altered during the frequency sweep.

The estimation accuracy (i.e., the MSE) of proposed frequency estimation approach surpasses the exhaustive search measurements within the same resolution and observation time (Fig. 9). In fact, the proposed procedure results in up to 100 times accuracy more than exhaustive search when the bandwidth of resonator is limited ($W_r < 0.1\pi$). However, it loses this advantage when the bandwidth is wider than 0.2π of the normalized frequency.

In the conducted experiments, it is shown that the sensor system has comparable performance with advanced VNA devices up to 20 percent methanol. Noting that as the contribution of methanol increases in the solution, the value of relative permittivity decreases causing the bandwidth to be widen. This is similar to the results achieved from the simulations.

For future works, the functionality of the proposed sensor system can be extended to also extract the information related to peak attenuation of the transmission response ($\min|S_{12}|$), providing the complex relative permittivity. Moreover, with more advanced frequency estimation algorithms, sensing the characteristics of the MUT can be facilitated further. Optimal transmitted signals can be designed and utilized for providing efficiency in time and frequency. In addition, in cases where permittivity of the MUT changes within a sensing cycle, suitable tracking algorithms can be applied.

Appendix I

The noise level is an important property of SDR systems, which is a function of the SDR noise floor and input power. As the propagation channel is not involved in the proposed sensor system, it is reasonable to assume the noise is negligible. However, for low-power applications and the resonators with low Q-factor, the additive noise in the received signal cannot be omitted from equation (13). In the following, we will discuss how to tackle high noise level scenarios.

The power of the received signal $y[m,\omega_n]$ in (13) can be obtained as

$$|y[m,\omega_n]|^2 = |x[m,n]H(\omega_n,m) + q[m,\omega_n]|^2. \qquad (46)$$

This can be seen as squared L2 norm of bivariate complex Gaussian distribution as $y[m,\omega_n] \sim CN(x[m,n]H(\omega_n,m),\sigma^2)$. Let us scale the $y[m,\omega_n]$ with the factor of $1/\sigma$, then $|y[m,\omega_n]/\sigma|^2$ has a noncentral chi-squared distribution $\chi^2(k,\lambda)$ [47], where parameters $k = 2$ and λ is

$$\lambda = \left(\frac{real\left(x[m,n]H(\omega_n,m)\right)}{\sigma}\right)^2 + \left(\frac{imag\left(x[m,n]H(\omega_n,m)\right)}{\sigma}\right)^2$$
$$\lambda = \frac{|x[m,n]H(\omega_n,m)|^2}{\sigma^2}. \qquad (47)$$

The mean of noncentral chi-squared distribution is defined as [47]

$$\mu \triangleq k + \lambda = 2 + \frac{|x[m,n]H(\omega_n, m)|^2}{\sigma^2}. \quad (48)$$

Assuming σ^2 is a deterministic value, we write the expectation of equation (46) as

$$\mathrm{E}(|y[m,\omega_n]|^2) = |x[m,n]H(\omega_n, m)|^2 + 2\sigma^2. \quad (49)$$

So, to obtain $|x[m,n]H(\omega_n, m)|^2$, it is required to repeat the identical transmission with the same parameters N and M. Then, instead of one vector signal $\boldsymbol{y}[\omega_n]$, we would have an average over all the observed signals (for a specific n). Also, to achieve an unbiased estimate, a prior knowledge about the variance of additive noise (σ^2) must be available.

REFERENCES

[1] M. G. Mayani, F. J. Herraiz-Martínez, J. M. Domingo, and R. Giannetti, "Resonator-based microwave metamaterial sensors for instrumentation: Survey, classification, and performance comparison," *IEEE Transactions on Instrumentation and Measurement*, vol. 70, pp. 1-14, 2020.

[2] A. Ebrahimi, J. Scott, and K. Ghorbani, "Ultrahigh-sensitivity microwave sensor for microfluidic complex permittivity measurement," *IEEE Transactions on Microwave Theory and Techniques*, vol. 67, no. 10, pp. 4269-4277, 2019.

[3] M. S. Boybay and O. M. Ramahi, "Material characterization using complementary split-ring resonators," *IEEE Transactions on instrumentation and Measurement*, vol. 61, no. 11, pp. 3039-3046, 2012.

[4] J. Shi *et al.*, "A 3D-Printed Flexible Radio Frequency Strain Sensor Based On Complementary Split Ring Resonator," *IEEE Sensors Journal*, 2022.

[5] M. U. Memon, A. Salim, H. Jeong, and S. Lim, "Metamaterial inspired radio frequency-based touchpad sensor system," *IEEE Transactions on Instrumentation and Measurement*, vol. 69, no. 4, pp. 1344-1352, 2019.

[6] C.-Z. Wu and C.-H. Tseng, "A perturbation-injection-locked sensor with self-oscillating active CSRR for vital-sign detection from fingertip," in *2019 IEEE MTT-S International Microwave Symposium (IMS)*, 2019: IEEE, pp. 369-372.

[7] C.-H. Tseng and C.-Z. Wu, "A novel microwave phased-and perturbation-injection-locked sensor with self-oscillating complementary split-ring resonator for finger and wrist pulse detection," *IEEE Transactions on Microwave Theory and Techniques*, vol. 68, no. 5, pp. 1933-1942, 2020.

[8] G. Govind and M. J. Akhtar, "Metamaterial-inspired microwave microfluidic sensor for glucose monitoring in aqueous solutions," *IEEE Sensors Journal*, vol. 19, no. 24, pp. 11900-11907, 2019.

[9] A. E. Omer *et al.*, "Non-invasive real-time monitoring of glucose level using novel microwave biosensor based on triple-pole CSRR," *IEEE Transactions on Biomedical Circuits and Systems*, vol. 14, no. 6, pp. 1407-1420, 2020.

[10] M. Abdolrazzaghi, N. Katchinskiy, A. Y. Elezzabi, P. E. Light, and M. Daneshmand, "Noninvasive glucose sensing in aqueous solutions using an active split-ring resonator," *IEEE Sensors Journal*, vol. 21, no. 17, pp. 18742-18755, 2021.

[11] G. Acevedo-Osorio, E. Reyes-Vera, and H. Lobato-Morales, "Dual-band microstrip resonant sensor for dielectric measurement of liquid materials," *IEEE Sensors Journal*, vol. 20, no. 22, pp. 13371-13378, 2020.

[12] O. Niksan, M. C. Jain, A. Shah, and M. H. Zarifi, "A Nonintrusive Flow Rate Sensor Based on Microwave Split-Ring Resonators and Thermal Modulation," *IEEE Transactions on Microwave Theory and Techniques*, vol. 70, no. 3, pp. 1954-1963, 2022.

[13] J. Xie, J. Wen, J. Chen, and W. Yuan, "Microwave Icing Sensor Based on Interdigital-Complementary Split-Ring Resonator," *IEEE Sensors Journal*, 2022.

[14] A. Rivera-Lavado, A. García-Lampérez, M.-E. Jara-Galán, E. Gallo-Valverde, P. Sanz, and D. Segovia-Vargas, "Low-Cost Electromagnetic Split-Ring Resonator Sensor System for the Petroleum Industry," *Sensors*, vol. 22, no. 9, p. 3345, 2022.

[15] P. Velez, J. Munoz-Enano, K. Grenier, J. Mata-Contreras, D. Dubuc, and F. Martín, "Split ring resonator-based microwave fluidic sensors for electrolyte concentration measurements," *IEEE Sensors Journal*, vol. 19, no. 7, pp. 2562-2569, 2018.

[16] P. Vélez, L. Su, K. Grenier, J. Mata-Contreras, D. Dubuc, and F. Martín, "Microwave microfluidic sensor based on a microstrip splitter/combiner configuration and split ring resonators (SRRs) for dielectric characterization of liquids," *IEEE Sensors Journal*, vol. 17, no. 20, pp. 6589-6598, 2017.

[17] E. L. Chuma, Y. Iano, G. Fontgalland, and L. L. B. Roger, "Microwave sensor for liquid dielectric characterization based on metamaterial complementary split ring resonator," *IEEE Sensors Journal*, vol. 18, no. 24, pp. 9978-9983, 2018.

[18] A. Javed, A. Arif, M. Zubair, M. Q. Mehmood, and K. Riaz, "A low-cost multiple complementary split-ring resonator-based microwave sensor for contactless dielectric characterization of liquids," *IEEE Sensors Journal*, vol. 20, no. 19, pp. 11326-11334, 2020.

[19] A. M. Albishi, S. A. Alshebeili, and O. M. Ramahi, "Three-dimensional split-ring resonators-based sensors for fluid detection," *IEEE Sensors Journal*, vol. 21, no. 7, pp. 9138-9147, 2021.

[20] M. Gil, P. Vélez, F. Aznar-Ballesta, J. Muñoz-Enano, and F. Martín, "Differential sensor based on electroinductive wave transmission lines for dielectric constant measurements and defect detection," *IEEE Transactions on Antennas and Propagation*, vol. 68, no. 3, pp. 1876-1886, 2019.

[21] X. Han *et al.*, "Microwave Sensor Loaded With Complementary Curved Ring Resonator (CCRR) for Material Permittivity Detection," *IEEE Sensors Journal*, 2022.

[22] A. Ebrahimi, J. Scott, and K. Ghorbani, "Differential sensors using microstrip lines loaded with two split-ring resonators," *IEEE Sensors Journal*, vol. 18, no. 14, pp. 5786-5793, 2018.

[23] A. Ebrahimi, J. Scott, and K. Ghorbani, "Transmission lines terminated with LC resonators for differential permittivity sensing," *IEEE Microwave and Wireless Components Letters*, vol. 28, no. 12, pp. 1149-1151, 2018.

[24] J. Krupka, "Frequency domain complex permittivity measurements at microwave frequencies," *Measurement Science and Technology*, vol. 17, no. 6, p. R55, 2006.

[25] O. Huber, T. Faseth, G. Magerl, and H. Arthaber, "Dielectric characterization of RF-printed circuit board materials by microstrip transmission lines and conductor-backed coplanar waveguides up to 110 GHz," *IEEE Transactions on Microwave Theory and Techniques*, vol. 66, no. 1, pp. 237-244, 2017.

[26] P. Velez, K. Grenier, J. Mata-Contreras, D. Dubuc, and F. Martín, "Highly-sensitive microwave sensors based on open complementary split ring resonators (OCSRRs) for dielectric characterization and solute concentration measurement in liquids," *Ieee Access*, vol. 6, pp. 48324-48338, 2018.

[27] M. Baghelani, O. Hasan-Nejad, and M. Daneshmand, "Highly sensitive microwave sensor for high precision sensing of water contamination in mineral oil," *IEEE Sensors Journal*, vol. 21, no. 12, pp. 13247-13254, 2021.

[28] M. I. Souza, A. F. Da Mota, V. M. Pepino, J. P. Carmo, and B.-H. V. Borges, "Multi-purpose microwave biosensor based on signal encoding technique and microfluidics for improved sensitivity," *IEEE Sensors Journal*, vol. 21, no. 4, pp. 4571-4581, 2020.

[29] S. A. Alotaibi, Y. Cui, and M. M. Tentzeris, "CSRR based sensors for relative permittivity measurement with improved and uniform sensitivity throughout [0.9–10.9] GHz band," *IEEE Sensors Journal*, vol. 20, no. 9, pp. 4667-4678, 2019.

[30] J. D. Baena *et al.*, "Equivalent-circuit models for split-ring resonators and complementary split-ring resonators coupled to planar transmission lines," *IEEE transactions on microwave theory and techniques*, vol. 53, no. 4, pp. 1451-1461, 2005.

[31] J. Naqui, M. Durán-Sindreu, and F. Martín, "Modeling split-ring resonator (SRR) and complementary split-ring resonator (CSRR) loaded transmission lines exhibiting cross-polarization effects," *IEEE Antennas and Wireless Propagation Letters*, vol. 12, pp. 178-181, 2013.

[32] A. M. Albishi and O. M. Ramahi, "Microwaves-based high sensitivity sensors for crack detection in metallic materials," *IEEE Transactions on Microwave Theory and Techniques*, vol. 65, no. 5, pp. 1864-1872, 2017.

[33] R. Mirzavand, M. M. Honari, and P. Mousavi, "High-resolution balanced microwave material sensor with extended dielectric range," *IEEE Transactions on Industrial Electronics*, vol. 64, no. 2, pp. 1552-1560, 2016.

[34] H. Saghlatoon, R. Mirzavand, M. M. Honari, and P. Mousavi, "Sensor antenna transmitter system for material detection in wireless-sensor-node applications," *IEEE Sensors Journal*, vol. 18, no. 21, pp. 8812-8819, 2018.

[35] E. Lourenço Chuma, Y. Iano, L. L. B. Roger, and G. Fontgalland, "Measuring dielectric properties by two methods using software-defined radio," *IET Science, Measurement & Technology*, vol. 13, no. 7, pp. 1003-1008, 2019.

[36] A. Raza, A. Jabbar, D. A. Sehrai, H. Atiq, and R. Ramzan, "SDR Based VNA for Characterization of RF Sensors and Circuits," in *2021 1st International Conference on Microwave, Antennas & Circuits (ICMAC)*, 2021: IEEE, pp. 1-4.

[37] X. Hui, T. B. Conroy, and E. C. Kan, "Multi-point near-field RF sensing of blood pressures and heartbeat dynamics," *IEEE Access*, vol. 8, pp. 89935-89945, 2020.

[38] J. Z. Bao, M. L. Swicord, and C. C. Davis, "Microwave dielectric characterization of binary mixtures of water, methanol, and ethanol," *The Journal of chemical physics*, vol. 104, no. 12, pp. 4441-4450, 1996.

[39] N. Kumar, M. Rawat, and K. Rawat, "Software-defined radio transceiver design using FPGA-based system-on-chip embedded platform with adaptive digital predistortion," *IEEE access*, vol. 8, pp. 214882-214893, 2020.

[40] D. Rife and R. Boorstyn, "Single tone parameter estimation from discrete-time observations," *IEEE Transactions on information theory*, vol. 20, no. 5, pp. 591-598, 1974.

[41] E. Aboutanios and B. Mulgrew, "Iterative frequency estimation by interpolation on Fourier coefficients," *IEEE Transactions on signal processing*, vol. 53, no. 4, pp. 1237-1242, 2005.

[42] A. V. Oppenheim, *Discrete-time signal processing*. Pearson Education India, 1999.

[43] A. Antoniou and W.-S. Lu, *Practical optimization*. Springer, 2007.

[44] H. Nornikman, B. H. Ahmad, M. Z. A. Abd Aziz, and A. Othman, "Effect of single complimentary split ring resonator structure on microstrip patch antenna design," in *2012 IEEE symposium on wireless technology and applications (iswta)*, 2012: IEEE, pp. 239-244.

[45] G. Galindo-Romera, F. J. Herraiz-Martínez, M. Gil, J. J. Martínez-Martínez, and D. Segovia-Vargas, "Submersible printed split-ring resonator-based sensor for thin-film detection and permittivity characterization," *IEEE Sensors journal*, vol. 16, no. 10, pp. 3587-3596, 2016.

[46] S.-C. Pei and C.-C. Tseng, "Complex adaptive IIR notch filter algorithm and its applications," *IEEE Transactions on Circuits and Systems II: Analog and Digital Signal Processing*, vol. 41, no. 2, pp. 158-163, 1994.

[47] M. K. Simon, "Digital communication over generalized fading channels: a unified approach to performance analysis," 2002.